Current Control of Grid-Tied *LCL*-VSI With a Sliding Mode Controller in a Multiloop Approach

Leandro Tomé Martins, Márcio Stefanello, *Member, IEEE*, Humberto Pinheiro, *Member, IEEE*, and Rodrigo Padilha Vieira, *Member, IEEE*

***Abstract*—Despite several studies and approaches, the design of current controllers for grid-connected converters via *LCL* filters is still a challenging task. This is mainly due to the parametric uncertainties and the grid background voltage distortions to which the system is submitted. In order to overcome these inherent system challenges, this paper proposes a multiloop control framework that simplifies the system dynamics of the overall circuit by splitting it in two equivalent sub-circuits. An inner loop is implemented as a fast sliding mode controller that controls the filter capacitor voltage in a fast and robust way. As a result, the plant, viewed by the outer loop, yields a voltage-controlled voltage source connected to the grid through an *L* filter. Thus, multiple resonant controllers are included in the state-space representation of this simplified system, allowing the design of a state-feedback controller in the outer loop for asymptotic tracking of the grid current with disturbance rejection of the grid background voltage. Here, a discrete linear quadratic regulator algorithm is used for designing the state-feedback gains. A simple design procedure is presented, as well as simulations and experimental results, to show the good performance of the proposed control scheme even under significant uncertainties and disturbances of the system.**

***Index Terms*—*LCL* filter, linear quadratic regulator, multiloop control, sliding mode control, state-feedback control.**

I. Introduction

PULSEWIDTH modulated inverters are extensively used to interface renewable energy sources (e.g., solar, wind, etc.) with the utility grid. In order to improve power quality, the switching harmonics resulting from the pulsewidth modulation (PWM) must be filtered out to meet the requirements imposed by specific standards, such as the IEEE 1547-2003, which specifies the limits for both low- and high-frequency harmonic contents [1], [2]. This is typically accomplished by using power filters. The most common choices are the inductive (*L*) and the

Manuscript received August 27, 2018; revised November 20, 2018 and January 25, 2019; accepted March 2, 2019. Date of publication March 17, 2019; date of current version September 6, 2019. This work was supported in part by the Coordenação de Aperfeiçoamento de Pessoal de Nível Superior – Brasil (CAPES/PROEX) - Finance Code 001, and in part by INCT-GD (CNPq processo 465640/2014-1, CAPES processo no. 23038.000776/2017-54 e FAPERGS 17/2551-0000517-1). Recommended for publication by Associate Editor C. N. M. Ho. *(Corresponding author: Leandro Tomé Martins.)*

L. T. Martins, H. Pinheiro, and R. P. Vieira are with Power Electronics and Control Research Group, Federal University of Santa Maria, Santa Maria 97105-900, Brazil (e-mail:

a PI controller is the proportional plus resonant (PR) controller, which consists of the introduction of high gains at selected frequencies in order to eliminate the steady-state error [23]. Other alternative control schemes are well explored in an attempt to improve the robustness of the overall system [24], [25]. For instance, adaptive control strategies [26], partial-state-feedback controllers, and full-state-feedback controllers [27], [28].

It is worth mentioning that most current control schemes with a single feedback loop are associated with an active damping technique resulting in a cascaded or multiloop control scheme [29]–[31]. However, they just use information of an extra filter variable in order to add/subtract the control action, thus, reproducing the behavior of a virtual impedance to suppress the filter resonance. A few papers in the literature report the use of an extra inner control loop, where an ancillary variable is fed back to this loop and the grid-side current is fed back to an outer control loop. In [32], a dual control loop is presented and the inner loop is designed to regulate the capacitor voltage by means of a H_∞ repetitive controller. The authors identify that the plant, in the outer loop point of view, can be modeled by an *L*-filter connected to the grid. The H_∞ repetitive controller is also used in an outer loop in order to regulate the gird current. He *et al.* [33] present a boundary control with a second-order switching surface to reduce the order of the plant viewed by a deadbeat controller. The boundary control is implemented in an inner loop to regulate the filter capacitor voltage and its reference is generated by the deadbeat controller, which is implemented in an outer loop and used to regulate the grid current. Although this paper proposes a very interesting approach and experimental results are used to validate it, the deadbeat controller in the outer loop is sensitive to the grid inductance variation. To overcome this problem, the authors propose an estimation algorithm for the grid inductance, increasing the complexity of the proposed scheme.

Following the previous discussions, this paper proposes a multiloop control strategy to regulate the current of a three-phase grid-connected inverter with an *LCL* filter. Through the implementation of an inner loop, the *LCL* circuit is split in an *LC* filter followed by an *L* filter. The filter capacitor voltage is the controlled variable in this inner loop. The *L* filter is emphasized because a current controller must be designed for asymptotic tracking and disturbance compensation. It will be demonstrated that the inner loop synthesizes a voltage-controlled voltage source. Thus, a simpler plant represented by the voltage-controlled voltage source and an *L*-filter is seen from the outer loop and the design procedure of the current controller is easier than the case where no extra loop is added. In this paper, a discrete-time state-feedback controller is chosen and implements the outer loop. Resonant controllers are embedded into the state-space model of the outer loop for asymptotic tracking of the injected current and compensation of the grid voltage effects. Here (without any loss of generality), the gains of the state feedback controller are designed through the discrete linear quadratic regulator (DLQR) algorithm. To implement the inner loop, a sliding mode controller (SMC) is designed to ensure a fast and reliable response of the capacitor voltage [34]. The SMC also allows the independent design of the inner and outer loops because it ensures that the inner loop is fast enough if compared to the outer loop. Simulation and experimental results are presented to verify the performance of the proposed control scheme and its effectiveness in rejecting grid inductance variation.

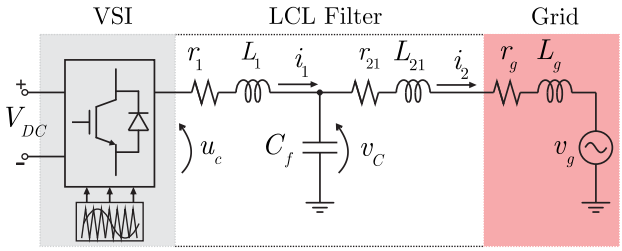

Fig. 1. Single-phase equivalent circuit of a grid-connected VSI with an *LCL* filter.

II. System Description

The system topology consists of a three-phase inverter with an *LCL* filter connected to the grid. The three-phase electric variables can be represented in the stationary reference frame through the $abc-\alpha\beta 0$ transformation. Thus, the three-phase circuit is represented by two decoupled single-phase circuits as shown in Fig. 1, since there is no circulating current for "0" axis. The single-phase circuit is used to obtain the plant model and some assumptions are made about the system: First, the grid is assumed as predominantly inductive and the inductance L_g is uncertain; second, the input voltage $V_{\rm DC}$ is obtained from an ideal dc source; and third, the synchronization with the grid voltage is ensured by using a Kalman filter, as presented in [35].

By defining the grid-side inductance as $L_2 = L_{21} + L_g$ and resistance as $r_2 = r_{21} + r_g$, the dynamic equations can be obtained by applying the Kirchhoff's law in the single-phase circuit of Fig. 1. The state-space representation results in

$$\begin{bmatrix} \dot{i}_1(t) \\ \dot{v}_C(t) \\ \dot{i}_2(t) \end{bmatrix} = \begin{bmatrix} -\frac{r_1}{L_1} & -\frac{1}{L_1} & 0 \\ \frac{1}{C_f} & 0 & -\frac{1}{C_f} \\ 0 & \frac{1}{L_2} & -\frac{r_2}{L_2} \end{bmatrix} \begin{bmatrix} i_1(t) \\ v_C(t) \\ i_2(t) \end{bmatrix} + \begin{bmatrix} \frac{1}{L_1} \\ 0 \\ 0 \end{bmatrix} u_c(t) + \begin{bmatrix} 0 \\ 0 \\ -\frac{1}{L_2} \end{bmatrix} v_g(t). \quad (1)$$

The switching effect of the PWM and its nonlinearity are neglected, thus the control action u_c is regarded itself as the voltage synthesized by the converter. The grid voltage v_g is considered a periodic disturbance. As the control algorithm is generally implemented in a digital signal processor based control platform, it is interesting to represent the plant model in the discrete-time domain [36]. Any discretization method can be used, however, in order to simplify the state-space model, Euler's discretization method is chosen. By applying Euler's method in (1), with a sampling period T_s, the discrete-time representation results in

$$\mathbf{x_d}_{(k+1)} = \mathbf{A_d}\mathbf{x_d}_{(k)} + \mathbf{B_d}u_{c(k)} + \mathbf{H_d}v_{g(k)} \quad (2)$$

where

$$\mathbf{A_d}=\begin{bmatrix} g_{11} & g_{12} & 0 \\ g_{21} & 1 & g_{23} \\ 0 & g_{32} & g_{33} \end{bmatrix}, \mathbf{B_d}=\begin{bmatrix} g_{14} \\ 0 \\ 0 \end{bmatrix}, \mathbf{H_d}=\begin{bmatrix} 0 \\ 0 \\ h_{d3} \end{bmatrix} \tag{3}$$

and $g_{11}=1-\frac{r_1}{L_1}T_s$, $g_{12}=-\frac{1}{L_1}T_s$, $g_{21}=\frac{1}{C_f}T_s$, $g_{23}=-\frac{1}{C_f}T_s$, $g_{32}=\frac{1}{L_2}T_s$, $g_{33}=1-\frac{r_2}{L_2}T_s$, $g_{14}=\frac{1}{L_1}T_s$, and $h_{d3}=-\frac{1}{L_2}T_s$.

In a digital system, the electric variables are sampled by analogue to digital converters and the control calculations are performed by a microcontroller. The control signals are compared with a triangular carrier to generate the PWM signals. This process introduces a time delay of one sample into the system, which can be accounted for in the state-space model as an extra state $\phi_{(k)}=u_{c(k-1)}$ [26], [37]. Including the one-sample time delay, the state-space representation (2) becomes

$$\begin{bmatrix} \mathbf{x_d}_{(k+1)} \\ \phi_{(k+1)} \end{bmatrix} = \begin{bmatrix} \mathbf{A_d} & \mathbf{B_d} \\ \mathbf{0}_{1\times 3} & 0 \end{bmatrix} \begin{bmatrix} \mathbf{x_d}_{(k)} \\ \phi_{(k)} \end{bmatrix} + \begin{bmatrix} \mathbf{0}_{1\times 3} \\ 1 \end{bmatrix} u_{c(k)} + \begin{bmatrix} \mathbf{H_d} \\ 0 \end{bmatrix} v_{g(k)} \tag{4}$$

which can be, likewise, written as

$$\mathbf{x_{dc}}_{(k+1)} = \mathbf{A_{dc}}\mathbf{x_{dc}}_{(k)} + \mathbf{B_{dc}}u_{c(k)} + \mathbf{H_{dc}}v_{g(k)} \tag{5}$$

with the state vector given by

$$\mathbf{x_{dc}}_{(k)} = \begin{bmatrix} i_{1(k)} & v_{C(k)} & i_{2(k)} & \phi_{(k)} \end{bmatrix}^{\intercal}. \tag{6}$$

III. Proposed Control Scheme

In this section, the proposed multiloop control scheme is presented. Two control loops are designed in order to allow simplification of the current control problem. The *LCL* filter system is split into two equivalent sub-circuits of reduced order, as shown in Fig. 2(a). Thus, an inner loop is implemented as a fast SMC that controls the filter capacitor voltage v_C. A state-feedback controller is used to control the injected grid current i_2 in the outer loop, which becomes simpler once the tracking of the capacitor voltage is ensured. The proposed control scheme is shown in Fig. 2(b) and a DLQR algorithm is used to design the state-feedback control gains. The overall system will be shown to be efficient in rejecting grid inductance variation. According to the theory of multiloop control, the dynamics of the inner control loop must be faster than that of the outer control loop. In this case, the two loops can be designed separately [32].

A. Inner Loop: SMC

The inner control loop is designed in order to ensure the tracking of the reference v_C^* of the filter capacitor voltage. For this reason, the tracking error $e_{(k)}=v_{C(k)}-v^*_{C(k)}$ is chosen as the switching function $\sigma_{(k)}$ [38]. From the theory of SMC, the sliding mode occurs when $\sigma_{(k)}=\sigma_{(k+1)}=0$, and by calculating the $\sigma_{(k+1)}$, one has

$$\sigma_{(k+1)} = v_{C(k+1)} - v^*_{C(k+1)}. \tag{7}$$

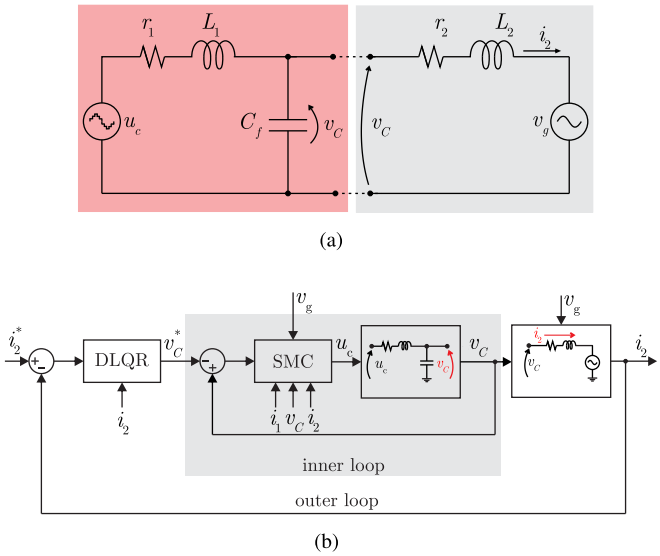

Fig. 2. (a) Circuit simplification obtained through a multiloop controller. (b) Proposed multiloop control scheme.

The value of $v_{C(k+1)}$ can be obtained by the state-space model (4) as follows:

$$\sigma_{(k+1)} = g_{21}i_{1(k)} + v_{C(k)} + g_{23}i_{2(k)} - v^*_{C(k+1)}. \tag{8}$$

From (8), one can verify that is not possible to synthesize the control law $u_{c(k)}$ by replacing $v_C(k+1)$ from the discrete-time model (4), i.e., there is a causality issue in this case. Due to this, the switching function is redefined as the tracking error two samples in advance, i.e.

$$\sigma_{(k)} = e_{(k+2)} = v_{C(k+2)} - v^*_{C(k+2)}. \tag{9}$$

Note that (9) requires information of the capacitor voltage and its reference two steps ahead. The estimate for $v_{C(k+2)}$ is obtained from the state-space representation (4), by solving for the state $v_{C(k)}$. Moreover, in order to obtain a causal control law, as it will be demonstrated, the reference v_C^* for the capacitor voltage must be delayed in three-sample time, which results in

$$\begin{aligned} \sigma_{(k)} = v_{C(k+2)} - v^*_{C(k-1)} &= s_1 i_{1(k)} + s_2 v_{C(k)} \\ &+ s_3 i_{2(k)} + s_4 \phi_{(k)} + s_5 v_{g(k)} - v^*_{C(k-1)} \end{aligned} \tag{10}$$

where $s_1=(g_{21}g_{11}+g_{21})$, $s_2=(g_{21}g_{12}+1+g_{23}g_{32})$, $s_3=(g_{23}+g_{23}g_{33})$, $s_4=g_{21}g_{14}$, and $s_5=g_{23}h_{d3}$.

The three-sample time delay in the reference of capacitor voltage causes a steady-state tracking error of the same three samples in the inner loop response, which will be compensated in the outer loop by taking into account the open-loop modeling.

From the theory of sliding mode control, the phase trajectory must start at any point of the phase plane and moves toward a switching line governed by the switching function and reaches this line in finite time [39]. This motion is called reaching mode. The equivalent form of the continuous reaching condition is not sufficient for the discrete SMC design. In [40], Gao *et al.* proposed a reaching law approach that dictates the dynamics of

the switching function for discrete-time systems. It is given by

$$\sigma_{(k+1)} = (1 - qT_s)\sigma_{(k)} - \varepsilon T_s \text{sign}(\sigma_{(k)}),\ \ 1 - qT_s > 0 \quad (11)$$

where ε and q are positive constants that are chosen in order to achieve a desirable reaching mode response.

The switching function one step ahead $\sigma_{(k+1)}$ in (11) is calculated from (10), which results in

$$\begin{aligned} s_1 i_{1(k+1)} + s_2 v_{C(k+1)} + s_3 i_{2(k+1)} + s_4 \phi_{(k+1)} \\ + s_5 v_{g(k+1)} - v^*_{C(k)} \\ = (1 - qT_s)\sigma_{(k)} - \varepsilon T_s \text{sign}(\sigma_{(k)}). \end{aligned} \quad (12)$$

The control law can be obtained from (12) by means of the term $\phi_{(k+1)} = u_{c(k)}$. The estimate of state variables one sample in advance $i_{1(k+1)}$, $v_{C(k+1)}$, and $i_{2(k+1)}$ can be obtained from the state-space model (4). Solving (12) for $u_{c(k)}$, the control law is obtained as follows:

$$\begin{aligned} u_{c(k)} = -\frac{1}{c_6}[c_1 i_{1(k)} + c_2 v_{C(k)} + c_3 i_{2(k)} + c_4 \phi_{(k)} + c_5 v_{g(k)} \\ + c_7 v_{g(k+1)} - v^*_{C(k)} + v^*_{C(k-1)} + qT_s \sigma_{(k)} + \varepsilon T_s \text{sign}(\sigma_{(k)})] \end{aligned} \quad (13)$$

where the constants are given by

$$\begin{aligned} c_1 &= (g_{21} g_{11} g_{11} + g_{21} g_{12} g_{21} + g_{23} g_{32} g_{21}) \\ c_2 &= (g_{21} g_{11} g_{12} + g_{21} g_{12} + g_{23} g_{32} + g_{23} g_{33} g_{32}) \\ c_3 &= (g_{21} g_{12} g_{23} + g_{23} g_{32} g_{23} + g_{23} g_{33} g_{33}) \\ c_4 &= g_{21} g_{11} g_{14},\ c_5 = g_{23} g_{33} h_{d3},\ c_6 = g_{21} g_{14}, \\ &\quad \text{and}\ c_7 = g_{23} h_{d3}. \end{aligned}$$

Notice that the control law is dependent on the actual and past sample times of the reference of capacitor voltage v^*_C only. This was possible by delaying the reference of capacitor voltage in the definition of switching function (10). Equation (13) is also dependent on the grid voltage one sample ahead $v_{g(k+1)}$. The value of v_g at a time instant $t = (k+1)T_s$ can be substituted by its value at $t = kT_s$ without compromising the inner control loop performance. This is possible because the small difference between the measured grid voltage and its next instant value remains insignificant, since, in practice, the grid voltage will never suffer from sudden variation over a sampling interval. Thus, the control law in (13) can be rewritten as follows:

$$\begin{aligned} u_{c(k)} = -\frac{1}{c_6}[c_1 i_{1(k)} + c_2 v_{C(k)} + c_3 i_{2(k)} + c_4 \phi_{(k)} \\ + (c_5 + c_7) v_{g(k)} - v^*_{C(k)} + v^*_{C(k-1)} \\ + qT_s \sigma_{(k)} + \varepsilon T_s \text{sign}(\sigma_{(k)})]. \end{aligned} \quad (14)$$

1) Closed-Loop Dynamics Analysis of the Inner Loop: The closed-loop dynamics of the inner loop can be evaluated by substituting the one-sample delayed control action $u_{c(k-1)} = \phi_{(k)}$ into the state-space model (4). By solving the state equations v_C and i_1 in (4), one has

$$v_{C(k+1)} = g_{21} i_{1(k)} + v_{C(k)} + g_{23} i_{2(k)} \quad (15)$$

and

$$\begin{aligned} i_{1(k+1)} \\ = g_{11} i_{1(k)} + g_{12} v_{C(k)} - \frac{1}{g_{21}}\big[c_1 i_{1(k-1)} + c_2 v_{C(k-1)} \\ + c_3 i_{2(k-1)} + c_4 \phi_{(k-1)} + (c_5 + sc_7) v_{g(k-1)} \\ - v^*_{C(k-1)} + v^*_{C(k-2)} + qT_s \sigma_{(k-1)} + \varepsilon T_s \text{sign}(\sigma_{(k-1)})\big]. \end{aligned} \quad (16)$$

Therefore, by delaying (16) by one-sample time and substituting it in (15), one has

$$\begin{aligned} v_{C(k+1)} = g_{21} g_{11} i_{1(k-1)} + g_{21} g_{12} v_{C(k-1)} - c_1 i_{1(k-2)} \\ - c_2 v_{C(k-2)} - c_3 i_{2(k-2)} - c_4 \phi_{(k-2)} \\ - (c_5 + c_7) v_{g(k-2)} + v^*_{C(k-2)} - v^*_{C(k-3)} - qT_s \sigma_{(k-2)} \\ - \varepsilon T_s \text{sign}\left(\sigma_{(k-2)}\right) + v_{C(k)} + g_{23} i_{2(k)}. \end{aligned} \quad (17)$$

Furthermore, a term $c_7 v_{g(k-1)}$ can be added and subtracted from (17) without compromising the authenticity of this equation. This operation is done in order to simplify the analysis of the closed inner loop dynamics. Thus, (17) is expressed as

$$\begin{aligned} v_{C(k+1)} = g_{21} g_{11} i_{1(k-1)} + g_{21} g_{12} v_{C(k-1)} \\ - c_1 i_{1(k-2)} - c_2 v_{C(k-2)} - c_3 i_{2(k-2)} - c_4 \phi_{(k-2)} \\ - (c_5 + c_7) v_{g(k-2)} + (c_7 - c_7)\, v_{g(k-1)} + v^*_{C(k-2)} \\ - v^*_{C(k-3)} - qT_s \sigma_{(k-2)} - \varepsilon T_s \text{sign}\left(\sigma_{(k-2)}\right) \\ + v_{C(k)} + g_{23} i_{2(k)}. \end{aligned} \quad (18)$$

Hence, (18) can be simplified by substituting the constants, which results in a reduced equation in the form of

$$\begin{aligned} v_{C(k+1)} = v_{C(k)} + v^*_{C(k-2)} - v^*_{C(k-3)} - qT_s \sigma_{(k-2)} \\ - \varepsilon T_s \text{sign}(\sigma_{(k-2)}) - g_{23} h_{d3} \left(v_{g(k-2)} - v_{g(k-1)}\right) \end{aligned} \quad (19)$$

where $\sigma_{(k-2)} = v_{C(k)} - v^*_{C(k-3)}$. The discrete-time transfer function can be obtained by applying $\mathcal{Z}$-Transform in (19), which results in

$$V_C(z) = z^{-3} V^*_C(z) + g_{23} h_{d3} \frac{z-1}{z^2 (z + qT_s - 1)} V_g(z) - d(z) \quad (20)$$

where $d(z) = \varepsilon T_s \text{sign}\,[V_C(z) - z^{-3} V_C(z)^*]/[z + (qT_s - 1)]$ is a switched signal considered as an input disturbance for the outer loop.

Notice that (20) includes a term dependent on the grid voltage v_g and associated to a digital filter $g_{23} h_{d3}$ $(z-1)/(z^2(z + qT_s - 1))$. The dynamics arise from the replacement of the grid voltage $v_{g(k+1)}$ one-sample ahead by its current value $v_{g(k)}$ in (14). The associated digital filter attenuates the grid voltage signal under -20 dB at low frequencies, so the second term of (20) ideally does not affect the performance of the inner loop. In addition, the switched signal $d(z)$ also presents a small associated magnitude (due to the multiplication factor εT_s) and it does not affect the behavior of the inner loop either. For these reasons, the inner loop can be ideally represented as

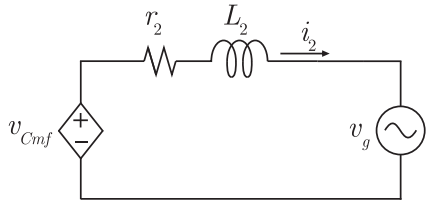

Fig. 3. Single-phase equivalent circuit obtained from simplification of system dynamics due to the control of v_C with the inner loop.

a perfect voltage-controlled voltage source $v_{Cmf(k)}$, which is given by

$$v_{Cmf(k)} = v^*_{C(k-3)}. \tag{21}$$

B. Outer Loop: State-Feedback Controller Using DLQR Algorithm

Once the closed inner loop dynamics (21) is obtained, the plant viewed by the outer loop is reduced to the equivalent circuit shown in Fig. 3, which consists of a voltage-controlled voltage source in series with the inductive filter $Z_2(s) = r_2 + L_2 s$ and the grid. Thus, an outer loop is designed in order to meet the following objectives: first, grid current tracking; second, rejection of the grid voltage distortions; and third, robustness with respect to parametric variation due to uncertain grid impedance.

1) Outer Open-Loop Model: The open-loop model of the simplified circuit is obtained by applying the Kirchhoff's law in the circuit of Fig. 3. The continuous-time differential equation that describes its dynamics results in

$$\frac{di_{2(t)}}{dt} = -\frac{r_2}{L_2} i_{2(t)} + \frac{1}{L_2} v_{Cmf(t)} - \frac{1}{L_2} v_{g(t)} \tag{22}$$

where $v_{Cmf(t)}$ is the output signal of the inner closed-loop control system given in (21). By applying the Laplace's transform in (22), the transfer function $G_{mi}(s)$ of the outer open-loop system, where the input is the output signal of the inner loop, is obtained as

$$G_{mi}(s) = \frac{I_{2(s)}}{V_{Cmf(s)}} = \frac{1/L_2}{s + r_2/L_2}. \tag{23}$$

Here, to represent (23) in the discrete-time domain, the *Tustin* method was used and the discrete-time transfer function $G_{mi}(z)$ was obtained as

$$G_{mi}(z) = \frac{I_2(z)}{z^{-3} V^*_C(z)} = G_{mi}(s)\Big|_{s=\frac{2}{T_s}\frac{z-1}{z+1}} \tag{24}$$

which can be, likewise, described by

$$G_{mi}(z) = z^{-3} k_{m1} \frac{(z+1)}{(z+p_{m1})} \tag{25}$$

where $k_{m1} = T_s/(2L_2 + r_2 T_s)$ and $p_{m1} = (r_2 T_s - 2L_2)/(2L_2 + r_2 T_s)$. One can note that the outer loop system is easier to control if compared to the original *LCL* system. The model (25) is simply composed by a delay z^{-3} due to the definition of the switching function on the inner loop design and a first-order system with one pole p_{m1} due to the *L* filter of the simplified circuit, which is the plant for the outer control loop.

The transfer function (25) can be alternatively represented by a state-space model in the discrete-time domain. Notice that this system includes a time-delay of three samples of the reference of the capacitor voltage, which results from the closed-loop dynamics of the inner loop (21). Thus, three states are defined to model this delay according to

$$\begin{cases} \phi_{1(k)} = v^*_{C(k-1)} \\ \phi_{2(k)} = \phi_{1(k-1)} = v^*_{C(k-2)} \\ \phi_{3(k)} = \phi_{2(k-1)} = v^*_{C(k-3)}. \end{cases} \tag{26}$$

Hence, from (25) and (26), it is possible to obtain the following discrete-time state-space model for the outer loop:

$$\begin{aligned} \mathbf{x_1}_{(k+1)} &= \tilde{\mathbf{A}}\mathbf{x_1}_{(k)} + \tilde{\mathbf{B}} v^*_{C(k)} + \tilde{\mathbf{H}} v_{g(k)} \\ y_{(k)} &= \tilde{\mathbf{C}}\mathbf{x_1}_{(k)} \end{aligned} \tag{27}$$

with $\tilde{\mathbf{A}} \in \mathbb{R}^{4\times4}$, $\tilde{\mathbf{B}} \in \mathbb{R}^{4\times1}$, $\tilde{\mathbf{H}} \in \mathbb{R}^{4\times1}$, and the output matrix $\tilde{\mathbf{C}} = [1\ \ 0\ \ 0\ \ 0]$. The state vector is given by

$$\mathbf{x_1}_{(k)} = \begin{bmatrix} i_{2(k)} & \phi_{1(k)} & \phi_{2(k)} & \phi_{3(k)} \end{bmatrix}^\intercal. \tag{28}$$

2) Inclusion of Resonant Controllers in the Outer Open-Loop Model: In order to achieve the control objectives stated above, resonant controllers are embedded in the outer open-loop model (27). This type of controller is based on the internal model principle and its discrete-time state-space representation is given by [28]

$$\boldsymbol{\xi}_{i(k+1)} = \mathbf{R}_i \boldsymbol{\xi}_{i(k)} + \mathbf{T}_i e_{(k)} \tag{29}$$

where $\boldsymbol{\xi}_{i(k)} \in \mathbb{R}^{2\times1}$, $\mathbf{R}_i \in \mathbb{R}^{2\times2}$, and $\mathbf{T}_i \in \mathbb{R}^{2\times1}$.

Note that (29) allows the deployment of j resonant controllers, each one for a specific desirable frequency i in order to track or reject sinusoidal signals. Thus, the augmented representation for j resonant controllers becomes

$$\boldsymbol{\xi}_{(k+1)} = \mathbf{R}\boldsymbol{\xi}_{(k)} - \mathbf{T}\tilde{\mathbf{C}}\mathbf{x_1}_{(k)} + \mathbf{T} i^*_{2(k)} \tag{30}$$

where

$$\begin{aligned} &\boldsymbol{\xi} = \begin{bmatrix} \boldsymbol{\xi}_1 & \dots & \boldsymbol{\xi}_j \end{bmatrix}^\intercal, \mathbf{R} = \text{diag}\begin{bmatrix} \mathbf{R_1} & \dots & \mathbf{R}_j \end{bmatrix}, \text{and} \\ &\mathbf{T} = \begin{bmatrix} \mathbf{T_1} & \dots & \mathbf{T}_j \end{bmatrix}^\intercal. \end{aligned} \tag{31}$$

The inclusion of multiple resonant controllers in the outer open-loop model given in (27) results in an augmented system that can be modeled as

$$\begin{aligned} \begin{bmatrix} \mathbf{x_1}_{(k+1)} \\ \boldsymbol{\xi}_{(k+1)} \end{bmatrix} &= \begin{bmatrix} \tilde{\mathbf{A}} & \mathbf{0}_{4\times2j} \\ -\mathbf{T}\tilde{\mathbf{C}} & \mathbf{R} \end{bmatrix} \begin{bmatrix} \mathbf{x_1}_{(k)} \\ \boldsymbol{\xi}_{(k)} \end{bmatrix} + \begin{bmatrix} \tilde{\mathbf{B}} \\ \mathbf{0}_{2j\times1} \end{bmatrix} v^*_{C(k)} \\ &+ \begin{bmatrix} \mathbf{0}_{4\times1} \\ \mathbf{T} \end{bmatrix} i^*_{2(k)} + \begin{bmatrix} \tilde{\mathbf{H}} \\ \mathbf{0}_{2j\times1} \end{bmatrix} v_{g(k)} \\ y_{(k)} &= \begin{bmatrix} \tilde{\mathbf{C}} & \mathbf{0}_{1\times2j} \end{bmatrix} \begin{bmatrix} \mathbf{x_1}_{(k)} \\ \boldsymbol{\xi}_{(k)} \end{bmatrix} \end{aligned} \tag{32}$$

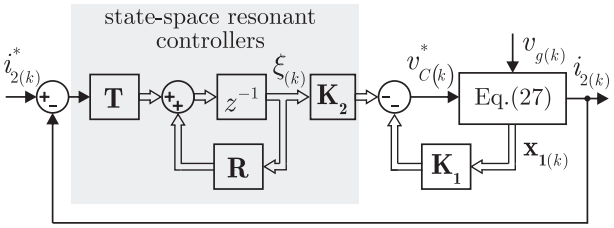

Fig. 4. State-feedback control for the outer loop including resonant controllers in the system model.

or in a compact form

$$\begin{aligned}\mathbf{x_{p}}_{(k+1)} &= \tilde{\mathbf{A}}_\mathbf{p}\mathbf{x_{p}}_{(k)} + \tilde{\mathbf{B}}_\mathbf{p}v^*_{C(k)} + \tilde{\mathbf{B}}_\mathbf{rp}i^*_{2(k)} + \tilde{\mathbf{H}}_\mathbf{p}v_{g(k)} \\ y_{(k)} &= \tilde{\mathbf{C}}_\mathbf{p}\mathbf{x_{p}}_{(k)}.\end{aligned} \tag{33}$$

The form (33) allows the design of all state-feedback gains simultaneously to be used in a state-feedback control law.

3) Design of the State-Feedback Controller: The state-feedback control law is given by

$$u_{(k)} = -\mathbf{K}\mathbf{x_{p}}_{(k)} \tag{34}$$

where $\mathbf{K} \in \mathbb{R}^{1\times(2j+4)}$. By using the DLQR algorithm, the gain vector $\mathbf{K}$ can be designed in such a way as to minimize a quadratic cost function given by

$$\mathscr{J} = \frac{1}{2}\sum_{k=1}^{\infty}[\mathbf{x}^\intercal_{\mathbf{p}(k)}\mathbf{Q_c}\mathbf{x_{p}}_{(k)} + u^\intercal{}_{(k)}\mathbf{R_c}u_{(k)}] \tag{35}$$

where $\mathbf{Q_c} > 0 \in \mathbb{R}^{(2j+4)}$, $\mathbf{R_c} > 0 \in \mathbb{R}$ are positive-definite matrices, and $\mathbf{Q_c}$ provides the importance of each state, whereas $\mathbf{R_c}$ weights the control signal leading to smaller amplitude as larger is its value.

From the theory of optimal control, the vector $\mathbf{K}$ has solution in the form of

$$\mathbf{K} = (\tilde{\mathbf{B}}^\intercal_\mathbf{p}\mathbf{P_c}\tilde{\mathbf{B}}_\mathbf{p} + \mathbf{R_c})^{-1}\tilde{\mathbf{B}}_\mathbf{p}\mathbf{P_c}\tilde{\mathbf{A}}_\mathbf{p} \tag{36}$$

where $\mathbf{P_c}$ is the solution of the Riccati's equation given by [41]

$$\begin{aligned}&\tilde{\mathbf{A}}^\intercal_\mathbf{p}\mathbf{P_c}\tilde{\mathbf{A}}_\mathbf{p} - \mathbf{P_c} - (\tilde{\mathbf{A}}^\intercal_\mathbf{p}\mathbf{P_c}\tilde{\mathbf{B}}_\mathbf{p})(\tilde{\mathbf{B}}^\intercal_\mathbf{p}\mathbf{P_c}\tilde{\mathbf{B}}_\mathbf{p}+\mathbf{R_c})^{-1}(\tilde{\mathbf{B}}^\intercal_\mathbf{p}\mathbf{P_c}\tilde{\mathbf{A}}_\mathbf{p}) \\ &+ \mathbf{Q_c} = 0.\end{aligned} \tag{37}$$

As the control law $u_{(k)}$ corresponds to capacitor voltage reference $v^*_{C(k)}$, (34) can be expressed as

$$v^*_{C(k)} = -\mathbf{K}\mathbf{x_{p}}_{(k)} \tag{38}$$

and the state-feedback gain vector is written as $\mathbf{K} = [\mathbf{K_1}\ \mathbf{K_2}]$, where $\mathbf{K_1} = [K_{i2}\ \ K_{\phi1}\ \ K_{\phi2}\ \ K_{\phi3}]$ and $\mathbf{K_2}$ is the gain vector associated to resonant controllers states. A closed-loop scheme for the outer loop is shown in Fig. 4.

IV. Design and Simulation

This section presents a design example of the proposed control scheme and the performance is assessed by simulation results.

TABLE I
System Parameters for Simulation and Experimental Results

Parameter	Value	Parameter	Value
L_1, r_1	1.0 mH, 0.5 Ω	f_s, f_{sw}	12000 Hz
L_{21}, r_{21}	0.3 mH, 0.5 Ω	ω_g	$2\pi60$ rad/s
C_f	62 μF	V_g (RMS)	110 V
L_g	[0 1.0] mH	I_2, ϕ^*_{i2}	7–14 A, 0°

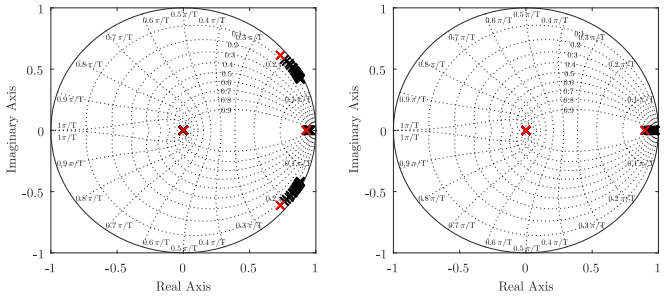

Fig. 5. Influence of the change in L_g, from 0 to 1 mH. Eigenvalues of (a) open-loop matrix $\mathbf{A_{dc}}$ and (b) matrix $\tilde{\mathbf{A}}$ of the simplified system after closing the loop with the SMC.

The plant parameters are given in Table I. Note that the parameter L_g comprehends a variation in the grid inductance, which is a typical situation in an uncertain grid.

A. Design Procedure

The design method is divided into two steps as follows.

1) Step I. Design of the Inner Loop: The design of SMC is based on the system parameters. First, the switching function $\sigma_{(k)}$ is obtained as presented in (10), and then, the control action $u_{c(k)}$ arises from (14). The constants $\varepsilon = 15000$ and $q = 11990$ were designed as outlined in [42]. To show the influence of the change of the grid inductance L_g, consider the pole zero maps in Fig. 5. The eigenvalues of matrix $\mathbf{A_{dc}}$ of the open-loop model (5) are shown in Fig. 5(a), whereas the outer open-loop model (27) yields in the eigenvalues of matrix $\tilde{\mathbf{A}}$ that are illustrated in Fig. 5(b). Notice that the eigenvalues associated to the systems models with minimum grid inductance $L_g = 0$ mH are represented in red. As L_g increases up to 1 mH, the eigenvalues are displaced according to the ones represented in black. This variation of grid inductance forces the poles of the system to move toward to the outside of the unit circle (unstable region). However, for the variation limits considered in this paper, the stability is ensured.

2) Step II. Design of the Outer Loop: According to Section III-B, the resonant controllers are embedded in the open-loop system of the simplified circuit model (27). Thus, the resonance frequencies ω_i for the fundamental, fifth, and seventh harmonics are chosen as presented in Table II, as well as their correspondent damping factors ζ_i. The discrete-time eigenvalues of the augmented system (33) are shown in Fig. 6(a). The closed-loop is achieved through the state-feedback controller and the gains are designed by the DLQR algorithm.

TABLE II
OUTER LOOP DESIGN PARAMETERS FOR SIMULATION AND EXPERIMENTAL RESULTS

Parameter	Value
	Resonant controllers parameters
$\omega_{1,5,7}$	60, 300, 420 Hz
$\zeta_{1,5,7}$	0.0001
	State-feedback DLQR input parameters
$\mathbf{Q_c}$	diag([500 1 1 1 10 10 50 50 50 50])
$\mathbf{R_c}$	10

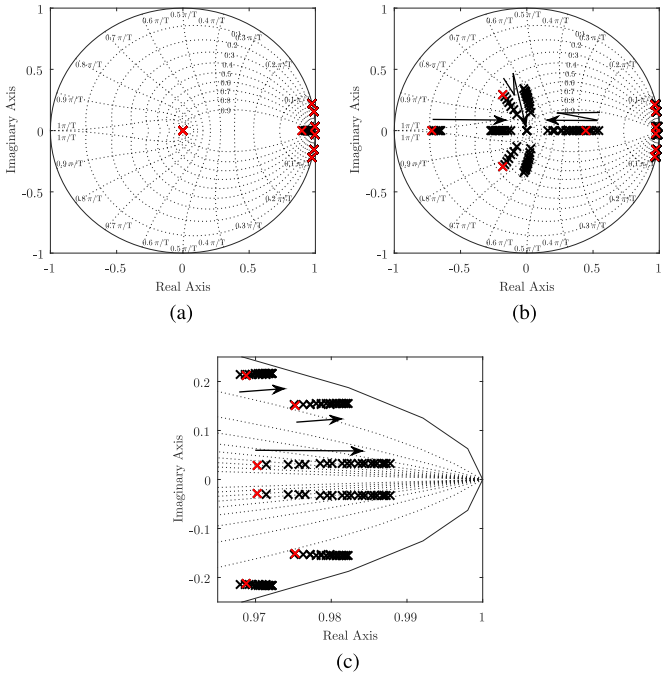

Fig. 6. Eigenvalues of (a) matrix $\tilde{\mathbf{A}}_\mathbf{p}$ of the open-loop augmented system and (b) matrix $(\tilde{\mathbf{A}}_\mathbf{p} - \tilde{\mathbf{B}}_\mathbf{p}\mathbf{K})$ of the closed-loop system, for $L_g \in [0\ \ 1]$ mH. (c) Zoom nearby the border of a unit circle with a closed-loop system.

For the given DLQR entries $\mathbf{Q_c}$ and $\mathbf{R_c}$ shown in Table II, the resulting gain vector of the state-feedback controller is $\mathbf{K} = [3.272\ \ 0.135\ \ 0.132\ \ 0.065\ \ -19.562\ \ 19.436\ \ -7.366\ \ 8.072\ \ -4.447\ \ 5.352]$.

The closed outer loop is assessed by the eigenvalues of matrix $(\tilde{\mathbf{A}}_\mathbf{p} - \tilde{\mathbf{B}}_\mathbf{p}\mathbf{K})$, and they are shown in Fig. 6(b) for $L_g \in [0\ 1]$ mH. The inherent system poles of the closed outer loop model move toward to the center of the unit circle as L_g increases, whereas the resonant poles move toward the outside of the unit circle. A zoom nearby the border of the unit circle is shown in Fig. 6(c), and the eigenvalues remain inside the circle for the variation limits considered in this paper. Thus, the stability of the closed outer loop is also ensured.

B. Analysis of the Simplified Outer Loop System Resulting From the Proposed Control Scheme

In this section, it is demonstrated that how the injected current control problem is simplified by adopting the proposed control scheme. As explained previously, the overall system is split into simplified circuits by controlling two filter variables separately. When the capacitor voltage is controlled in an inner loop, the outer open-loop representation yields in the circuit of Fig. 3. This circuit is modeled by (25), which results in

$$G_{mi}(z) = 0.1316\frac{(z+1)}{z^3(z-0.8947)} \tag{39}$$

considering $L_g = 0$ mH. The frequency response of the outer open-loop system is shown in Fig. 7(a). One can notice that the magnitude plot presents a -20 dB/dec decay at approximately 30 Hz and that there is no resonance peak. Furthermore, the inner loop is considered to be a voltage-controlled voltage source with the three-sample time delay being the dynamics associated to this source. In this regard, the first-order filter in series with this controlled voltage source results in a simpler system to be controlled if compared to the original system using a single control loop. The frequency response in Fig. 7(b) shows that controlled outer loop system compensates the fundamental, fifth-order harmonics, and seventh-order harmonics signals.

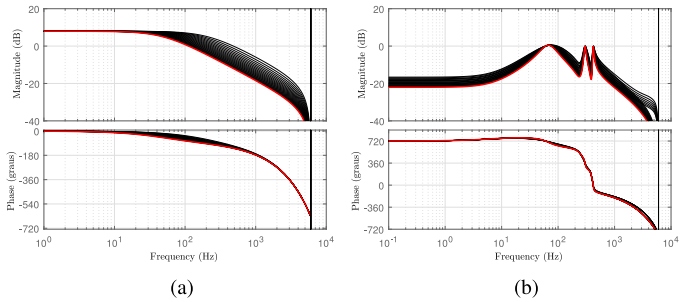

Fig. 7. Frequency response of (a) outer open-loop system (25) and (b) outer closed-loop system.

C. Simulation Results

The simulations were performed using a simulation software. The system parameters are given in Table I and the grid current references are $i^*_{2\alpha} = I_2 \sin(\omega_g t + \phi_{i^*_{2\alpha}})$ and $i^*_{2\beta} = I_2 \cos(\omega_g t + \phi_{i^*_{2\beta}})$.

The results for a variation of the reference of the grid current i^*_2 are shown on Fig. 8. The grid current $i_{2\alpha}$ for the α-axis shows the good tracking performance for the amplitude variation of 0–7 A at 0.0166 s and from 7 to 14 A at 0.0667 s. The error between the injected grid current and its reference $e_{i2\alpha}$ for the α-axis emphasizes the tracking performance and the fast response of the proposed control scheme. Besides, it is demonstrated that the grid current is not affected by a grid voltage distortion. In this case, the grid was simulated with the fifth and seventh voltage harmonics with amplitudes of 7.5% and 6.5% of the fundamental amplitude, respectively, and these distortions are fully eliminated by the outer control loop.

The inner loop is assessed by the waveform of capacitor voltage $v_{C\alpha}$, which demonstrates a good tracking performance in Fig. 8. This feature is emphasized by the waveform of the switching function σ_α for the α-axis. The chattering in the control action $u_{c\alpha}$ is due to the discontinuity inherent of the SMC and it

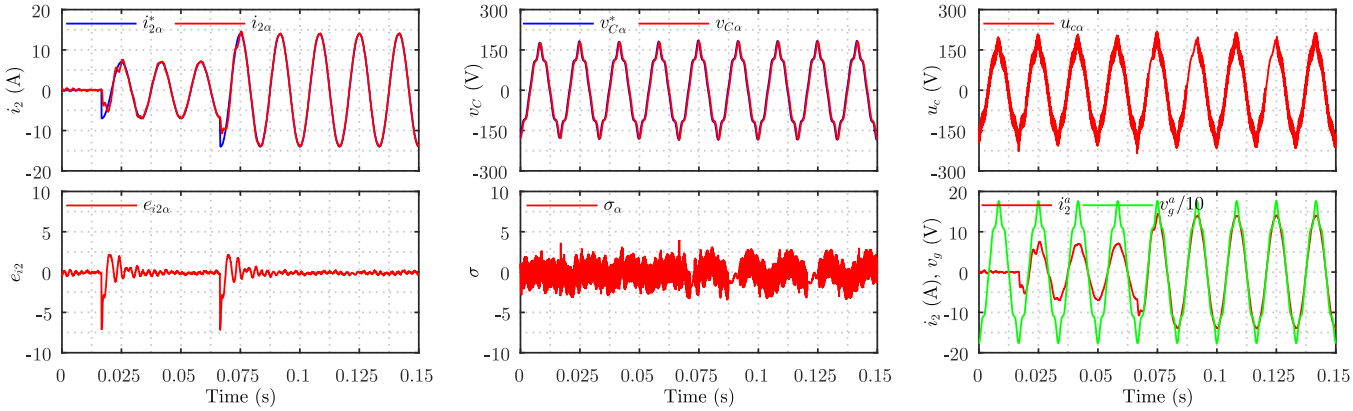

Fig. 8. Simulation results for variation of the reference of grid current i_2^*.

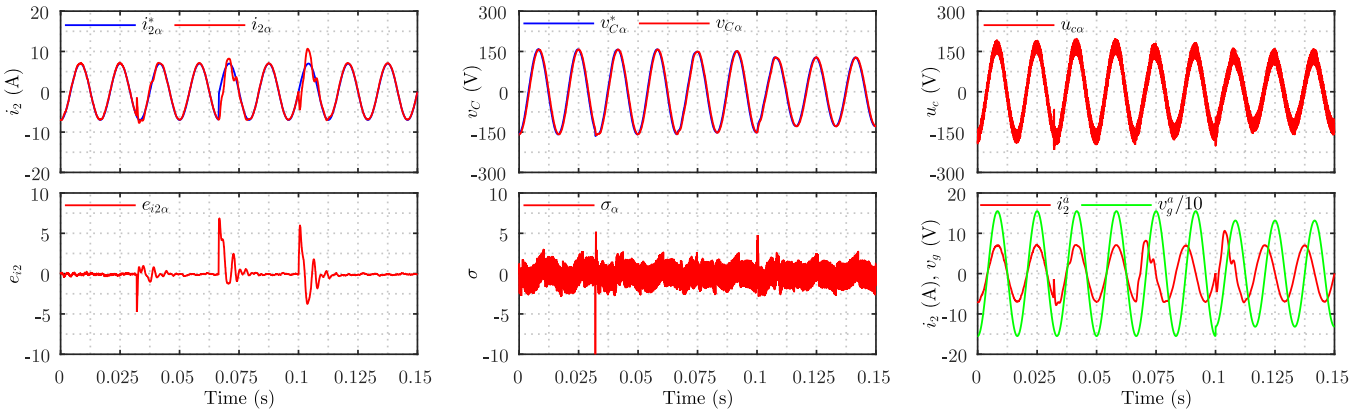

Fig. 9. Simulation results for variation of L_g, variation of grid current reference angles $\phi_{i_{2\alpha}^*}$ and $\phi_{i_{2\beta}^*}$, and variation of the grid voltage amplitude.

can be designed through the ε parameter as compromise between robustness and performance [42].

The results in Fig. 9 exhibit the effectiveness of the proposed control scheme in controlling the system even under variations of the grid inductance L_g, the grid reference current angles ($\phi_{i_{2\alpha}^*}$ and $\phi_{i_{2\beta}^*}$), and the grid voltage amplitude V_g. At 0.0333 s the inductance L_g is changed from 0 to 1 mH. Notice that the behavior of both, inner and outer loops, are barely affected by this variation. This demonstrates the capability of this proposed scheme in controlling the system even with different values of grid inductance. At 0.0667 s, the grid current references are lead with respect to the grid voltage, in such a way that the system provides reactive power to the grid. Finally, at 0.116 s, the grid voltage amplitude is decreased to 15% of its nominal value. Under these conditions, the grid current shows a transient perturbation that is briefly corrected and the capacitor voltage presents a minor variation.

D. Comparison Between the Proposed Control Scheme and a Conventional Controller

In order to evaluate the proposed control algorithm, a comparison with a conventional state-feedback controller is performed. This control technique was chosen for comparison purpose because its design and simplicity are well known in the literature [37], [43], [44]. The control law is defined as

$$u_{c(k)} = -\mathbf{K_i}\mathbf{x_i}_{(k)} \tag{40}$$

where $\mathbf{K_i} = [K_{i1} \quad K_{vC} \quad K_{i2} \quad K_\phi \quad \vdots \quad \mathbf{K_{i2}}]$ is the state-feedback gain vector. The state vector $\mathbf{x_i}_{(k)}$ is composed of the open-loop system states (5) and the states due to the resonant controllers (30) embedded into the open-loop system. The control algorithm is implemented as shown in Fig. 10 and the state-feedback gain vector is designed through the DLQR algorithm on MATLAB, which results in $\mathbf{K_i} = [3.248 \;\; 0.332 \;\; 1.192 \;\; 0.259 \;\; -26.989 \;\; 26.153 \;\; -9.752 \;\; 10.321 \;\; -6.926 \;\; 7.487]$.

To demonstrate the performance of both conventional and proposed controller schemes, a fictitious variation of the grid inductance from $L_g = 0$ to $L_g = 5$ mH is applied at 0.032 s in a simulation software. Fig. 11 shows the eigenvalues of the closed-loop systems considering both strategies under grid inductance variation. One can see that the eigenvalues of the proposed control scheme are much more damped if compared to the

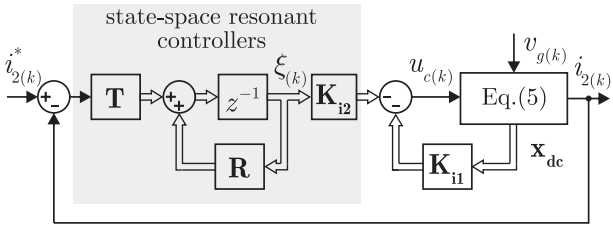

Fig. 10. State-feedback conventional control designed to compare with the proposed scheme.

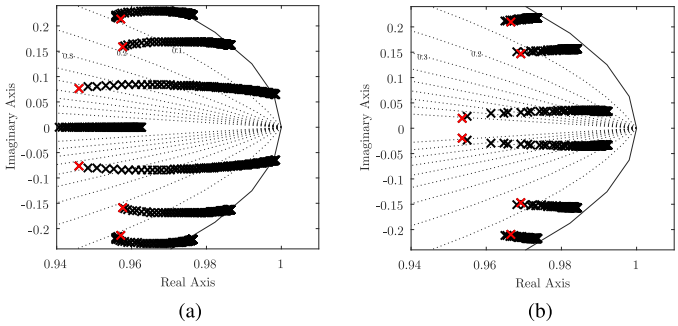

Fig. 11. Eigenvalues of closed-loop systems with (a) conventional state-feedback controller and (b) proposed control scheme.

eigenvalues of the conventional controller. This is due to the simplification of the circuit for designing the outer loop, where part of the *LCL* circuit is replaced by a voltage-controlled voltage source, resulting in an *L*-filter equivalent circuit to be current controlled (see Fig. 3).

Fig. 12 shows simulation results for closed-loop systems with the conventional and proposed control approaches. When the grid inductance varies, the conventional controller is not able to control the grid current because the system becomes unstable, whereas the proposed control scheme is still working properly. This emphasizes that the proposed control scheme is much more insensitive to the *LCL* resonance frequency variation.

V. Experimental Results

A laboratory prototype of a three-phase VSI with an *LCL* filter was used to evaluate the performance of the proposed control scheme in a real scenario, even for uncertain grid inductance values. The setup is shown in Fig. 15 and the system parameters are the same of those used to obtain the simulation results given in Table I. A voltage source was set at 450 V to provide a stable dc bus and the inverter with an output *LCL* filter is connected to the grid through a variable transformer. The control algorithm was programmed in C language in a DSP (TMS320F28335) from Texas Instruments.

The experimental results for variation of the reference i_2^* of the grid current obtained from the DSP data memory are presented in Fig. 13, just as the oscilloscope measurements are shown in Fig. 16(a). The reference is changed from 0 to 7 A at 0.0166 s and from 7 to 14 A at 0.0667 s. The inner loop presents

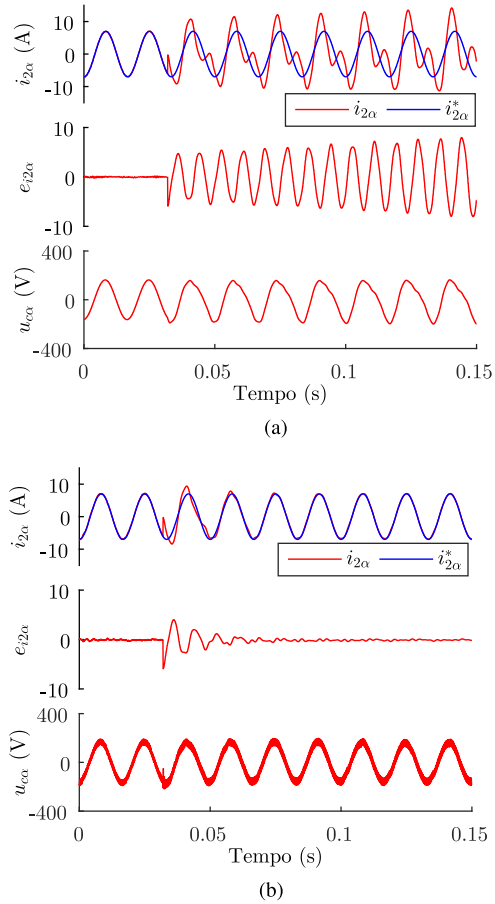

Fig. 12. Simulation results for the closed-loop system with (a) conventional state-feedback controller and (b) proposed control scheme.

a small tracking error as noticed from the waveforms of the filter capacitor voltage $v_{C\alpha}$ and the switching function σ_α for the α-axis. This error is associated to practical uncertainties in the real filter parameters. However, it does not affect the performance of the outer control loop, as the waveforms of the grid current i_2 and its associated tracking error e_{i2} demonstrate. The result for the α-axis of the grid current shows the good tracking performance of the outer loop and its fast response capacity.

To verify the effectiveness of the proposed scheme in controlling the system with an uncertain value of grid inductance, a switch is opened at 0.0333 s and an additional inductance is connected in series with the grid-side filter inductor L_{21}. This represents a change from 0 to 1 mH in the grid inductance L_g. The oscilloscope measurements shown in Fig. 16(b) and the DSP data memory plots shown in Fig. 14 highlight the good performance of the outer loop and its fast recovery capacity. The control scheme is shown to operate in a wide range of grid inductances values without compromising the closed-loop performance. Again, there is a small tracking error of the capacitor voltage in the inner loop due to uncertainties in the filter parameters; however, the performance of the injected grid current control is not affected. Furthermore, the reference angles $\phi_{i^*_{2\alpha}}$

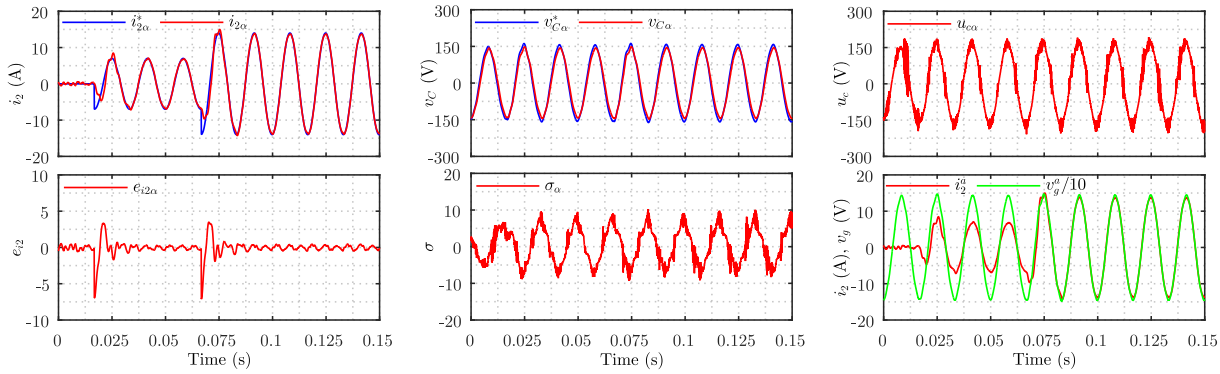

Fig. 13. Experimental results for variation of the reference of grid current i_2^*

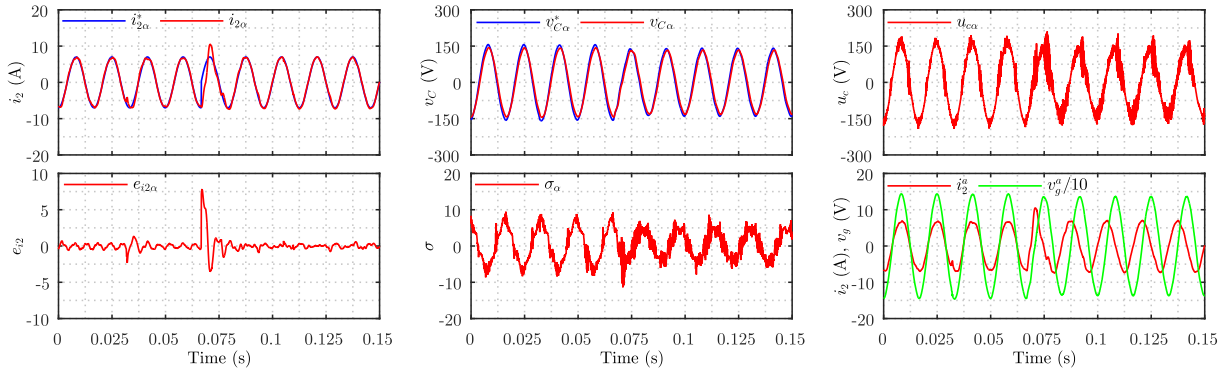

Fig. 14. Experimental results for variation of the grid inductance L_g and variation of grid current reference angles $\phi_{i_{2\alpha}^*}$ and $\phi_{i_{2\beta}^*}$.

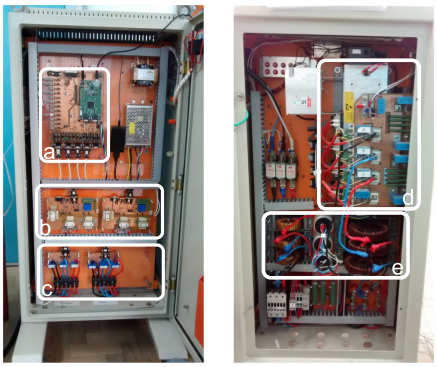

Fig. 15. Experimental setup. (a) DSP platform and signal conditioning circuits. (b) Voltage sensors with voltage transformers. (c) Current Hall-effect sensors. (d) Three-phase inverter with Semikron switches. (e) *LCL* filter.

and $\phi_{i_{2\beta}^*}$ of the injected grid current are put in advance with regard of the grid voltage, which corresponds to a typical situation of injecting reactive power into the grid. A comparison between the injected grid current and the grid voltage for the phase a shows the change in the grid current phase at 0.0667 s. A THD of 3.46% was measured, which shows that the proposed control scheme complies with IEEE standards.

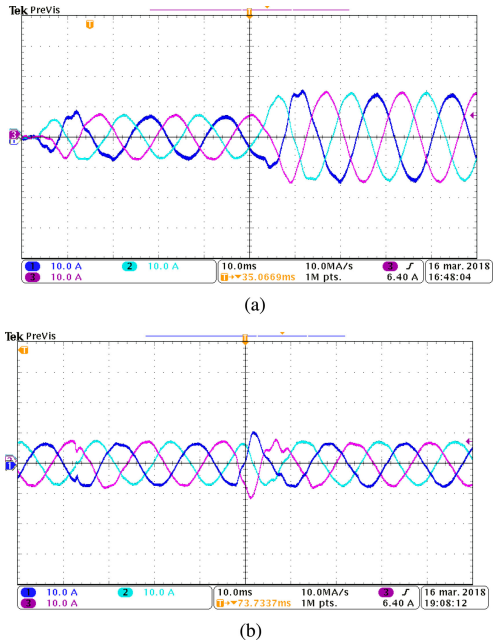

Fig. 16. Three-phase grid currents with (a) variation of grid current reference and (b) variation of L_g and grid current reference angles.

VI. Conclusion

The main feature of the proposed multiloop control strategy lies on the fact that the controls of filter capacitor voltage and grid current are nearly decoupled. Thus, the robustness of the overall system is enhanced, since parameter variations and disturbances are compensated in each control loop. A fast inner loop is designed through a SMC, allowing the outer loop to be designed separately. As a result, the plant viewed by the outer loop is simply modeled by a voltage-controlled voltage source with an L filter connected to the grid. State-space resonant controllers are embedded into the outer open-loop system and a state-feedback controller is designed through a DLQR algorithm.

Through a comparison analysis with a conventional controller, the proposed approach is showed to be much more insensitive to parametric variation. This is endorsed by the closed-loop eigenvalues analysis, in which the proposed control scheme presents much more damped eigenvalues than the conventional state-feedback controller. Simulation and experimental results demonstrated the good performance of the proposed control scheme even for an uncertain grid inductance condition, as well as a fast recovery capability from sudden changes in the reference and grid inductance.

References

[1] R. N. Beres, X. Wang, M. Liserre, F. Blaabjerg, and C. L. Bak, "A review of passive power filters for three-phase grid-connected voltage-source converters," *IEEE J. Emerg. Sel. Topics Power Electron*, vol. 4, no. 1, pp. 54–69, Mar. 2016.

[2] *IEEE Standard for Interconnecting Distributed Resources With Electric Power Systems*, IEEE Std 1547-2003, Jul. 2003.

[3] M. Liserre, F. Blaabjerg, and R. Teodorescu, "Grid impedance estimation via excitation of LCL-filter resonance," *IEEE Trans. Ind. Appl.*, vol. 43, no. 5, pp. 1401–1407, Sep. 2007.

[4] M. Liserre, F. Blaabjerg, and S. Hansen, "Design and control of an LCL-filter-based three-phase active rectifier," *IEEE Trans. Ind. Appl.*, vol. 41, no. 5, pp. 1281–1291, Sep./Oct. 2005.

[5] Y. Tang, W. Yao, P. C. Loh, and F. Blaabjerg, "Design of LCL filters with LCL resonance frequencies beyond the Nyquist frequency for grid-connected converters," *IEEE J. Emerg. Sel. Topics Power Electron.*, vol. 4, no. 1, pp. 3–14, Mar. 2016.

[6] R. N. Beres, X. Wang, F. Blaabjerg, M. Liserre, and C. L. Bak, "Optimal design of high-order passive-damped filters for grid-connected applications," *IEEE Trans. Power Electron.*, vol. 31, no. 3, pp. 2083–2098, Mar. 2016.

[7] R. Peña-Alzola, M. Liserre, F. Blaabjerg, R. Sebastián, J. Dannehl, and F. W. Fuchs, "Analysis of the passive damping losses in LCL-filter-based grid converters," *IEEE Trans. Power Electron.*, vol. 28, no. 6, pp. 2642–2646, Jun. 2013.

[8] W. Wu, Y. Liu, Y. He, H. S. H. Chung, M. Liserre, and F. Blaabjerg, "Damping methods for resonances caused by LCL-filter-based current-controlled grid-tied power inverters: An overview," *IEEE Trans. Ind. Electron.*, vol. 64, no. 9, pp. 7402–7413, Sep. 2017.

[9] J. Dannehl, F. W. Fuchs, S. Hansen, and P. B. Thogersen, "Investigation of active damping approaches for PI-based current control of grid-connected pulse width modulation converters with LCL filters," *IEEE Trans. Ind. Appl.*, vol. 46, no. 4, pp. 1509–1517, Jul. 2010.

[10] D. Pan, X. Ruan, C. Bao, W. Li, and X. Wang, "Capacitor-current-feedback active damping with reduced computation delay for improving robustness of LCL-type grid-connected inverter," *IEEE Trans. Power Electron.*, vol. 29, no. 7, pp. 3414–3427, Jul. 2014.

[11] C. Bao, X. Ruan, X. Wang, W. Li, D. Pan, and K. Weng, "Step-by-Step controller design for LCL-type grid-connected inverter with capacitor current-feedback active-damping," *IEEE Trans. Power Electron.*, vol. 29, no. 3, pp. 1239–1253, Mar. 2014.

[12] Z. Xin, P. C. Loh, X. Wang, F. Blaabjerg, and Y. Tang, "Highly accurate derivatives for LCL-filtered grid converter with capacitor voltage active damping," *IEEE Trans. Power Electron.*, vol. 31, no. 5, pp. 3612–3625, May 2016.

[13] R. Peña-Alzola, M. Liserre, F. Blaabjerg, R. Sebastin, J. Dannehl, and F. W. Fuchs, "Systematic design of the lead-lag network method for active damping in LCL-filter based three phase converters," *IEEE Trans. Ind. Inform.*, vol. 10, no. 1, pp. 43–52, Feb. 2014.

[14] X. Wang, F. Blaabjerg, and P. C. Loh, "Virtual RC damping of LCL-filtered voltage source converters with extended selective harmonic compensation," *IEEE Trans. Power Electron.*, vol. 30, no. 9, pp. 4726–4737, Sep. 2015.

[15] X. Wang, F. Blaabjerg, and P. C. Loh, "Grid-current-feedback active damping for LCL resonance in grid-connected voltage-source converters," *IEEE Trans. Power Electron.*, vol. 31, no. 1, pp. 213–223, Jan. 2016.

[16] Z. Xin, X. Wang, P. C. Loh, and F. Blaabjerg, "Grid-current-feedback control for LCL-filtered grid converters with enhanced stability," *IEEE Trans. Power Electron.*, vol. 32, no. 4, pp. 3216–3228, Apr. 2017.

[17] J. Yin, S. Duan, and B. Liu, "Stability analysis of grid-connected inverter with LCL filter adopting a digital single-loop controller with inherent damping characteristic," *IEEE Trans. Ind. Inform.*, vol. 9, no. 2, pp. 1104–1112, May 2013.

[18] M. Liserre, R. Teodorescu, and F. Blaabjerg, "Stability of photovoltaic and wind turbine grid-connected inverters for a large set of grid impedance values," *IEEE Trans. Power Electron.*, vol. 21, no. 1, pp. 263–272, Jan. 2006.

[19] D. Pan, X. Ruan, X. Wang, H. Yu, and Z. Xing, "Analysis and design of current control schemes for LCL-type grid-connected inverter based on a general mathematical model," *IEEE Trans. Power Electron.*, vol. 32, no. 6, pp. 4395–4410, Jun. 2017.

[20] F. Blaabjerg, R. Teodorescu, M. Liserre, and A. V. Timbus, "Overview of control and grid synchronization for distributed power generation systems," *IEEE Trans. Ind. Electron.*, vol. 53, no. 5, pp. 1398–1409, Oct. 2006.

[21] E. Twining and D. G. Holmes, "Grid current regulation of a three-phase voltage source inverter with an LCL input filter," *IEEE Trans. Power Electron.*, vol. 18, no. 3, pp. 888–895, May 2003.

[22] J. Dannehl, C. Wessels, and F. W. Fuchs, "Limitations of voltage-oriented PI current control of grid-connected PWM rectifiers with LCL Filters," *IEEE Trans. Ind. Electron.*, vol. 56, no. 2, pp. 380–388, Feb. 2009.

[23] R. Teodorescu, F. Blaabjerg, M. Liserre, and P. C. Loh, "Proportional-resonant controllers and filters for grid-connected voltage-source converters," *IEE Proc. Elect. Power Appl.*, vol. 153, no. 5, pp. 750–762, Sep. 2006.

[24] M. Andresen, M. Liserre, F. W. Fuchs, and N. Hoffmann, "Design of a grid adaptive controller for PWM converters with LCL filters," in *Proc. 41st Annu. Conf. IEEE Ind. Electron. Soc.*, Nov. 2015, pp. 003664–003671.

[25] F. Fuchs, J. Dannehl, and F. W. Fuchs, "Discrete sliding mode current control of grid-connected three-phase PWM converters with LCL filter," in *Proc. IEEE Int. Symp. Ind. Electron.*, Jul. 2010, pp. 779–785.

[26] J. R. Massing, M. Stefanello, H. A. Grundling, and H. Pinheiro, "Adaptive current control for grid-connected converters with LCL filter," *IEEE Trans. Ind. Electron.*, vol. 59, no. 12, pp. 4681–4693, Dec. 2012.

[27] I. J. Gabe, V. F. Montagner, and H. Pinheiro, "Design and implementation of a robust current controller for VSI connected to the grid through an LCL filter," *IEEE Trans. Power Electron.*, vol. 24, no. 6, pp. 1444–1452, Jun. 2009.

[28] L. A. Maccari *et al.*, "LMI-based control for grid-connected converters with LCL filters under uncertain parameters," *IEEE Trans. Power Electron.*, vol. 29, no. 7, pp. 3776–3785, Jul. 2014.

[29] P. C. Loh and D. G. Holmes, "Analysis of multiloop control strategies for LC/CL/LCL-filtered voltage-source and current-source inverters," *IEEE Trans. Ind. Appl.*, vol. 41, no. 2, pp. 644–654, Mar. 2005.

[30] Y. Jia, J. Zhao, and X. Fu, "Direct grid current control of LCL-filtered grid-connected inverter mitigating grid voltage disturbance," *IEEE Trans. Power Electron.*, vol. 29, no. 3, pp. 1532–1541, Mar. 2014.

[31] R. P. Vieira, L. T. Martins, J. R. Massing, and M. Stefanello, "Sliding mode controller in a multiloop framework for a grid-connected VSI with LCL filter," *IEEE Trans. Ind. Electron.*, vol. 65, no. 6, pp. 4714–4723, Jun. 2018.

[32] Q. C. Zhong and T. Hornik, "Cascaded current-voltage control to improve the power quality for a grid-connected inverter with a local load," *IEEE Trans. Ind. Electron.*, vol. 60, no. 4, pp. 1344–1355, Apr. 2013.

[33] Y. He, H. S. Chung, C. N. Ho, and W. Wu, "Use of boundary control with second-order switching surface to reduce the system order for deadbeat controller in grid-connected inverter," *IEEE Trans. Power Electron.*, vol. 31, no. 3, pp. 2638–2653, Mar. 2016.
[34] V. I. Utkin, J. Guldner, and J. Shi, *Sliding Mode Control in Electromechanical Systems*, 1st ed. New York, NY, USA: Taylor & Francis, 1999.
[35] R. Cardoso, R. F. D. Camargo, H. Pinheiro, and H. A. Grundling, "Kalman filter based synchronisation methods," *IET Gener., Transm. Distrib.*, vol. 2, no. 4, pp. 542–555, Jul. 2008.
[36] J. Wang, J. D. Yan, L. Jiang, and J. Zou, "Delay-dependent stability of single-loop controlled grid-connected inverters with LCL filters," *IEEE Trans. Power Electron.*, vol. 31, no. 1, pp. 743–757, Jan. 2016.
[37] J. Dannehl, F. W. Fuchs, and P. B. Thogersen, "PI state space current control of grid-connected PWM converters with LCL filters," *IEEE Trans. Power Electron.*, vol. 25, no. 9, pp. 2320–2330, Sep. 2010.
[38] Slotine, *Applied Nonlinear Control*. Englewood Cliffs, NJ, USA: Prentice-Hall, 1991.
[39] J. Y. Hung, W. Gao, and J. C. Hung, "Variable structure control: A survey," *IEEE Trans. Ind. Electron.*, vol. 40, no. 1, pp. 2–22, Feb. 1993.
[40] W. Gao, Y. Wang, and A. Homaifa, "Discrete-time variable structure control systems," *IEEE Trans. Ind. Electron.*, vol. 42, no. 2, pp. 117–122, Apr. 1995.
[41] S. Bittanti, *The Riccati Equation*. Berlin, Germany: Springer, 1991.
[42] G. S. Silva, R. P. Vieira, and C. Rech, "Discrete-time sliding-mode observer for capacitor voltage control in modular multilevel converters," *IEEE Trans. Ind. Electron.*, vol. 65, no. 1, pp. 876–886, Jan. 2017.
[43] F. Huerta, D. Pizarro, S. Cobreces, F. J. Rodriguez, C. Giron, and A. Rodriguez, "LQG servo controller for the current control of LCL grid-connected voltage-source converters," *IEEE Trans. Ind. Electron.*, vol. 59, no. 11, pp. 4272–4284, Nov. 2012.
[44] H. Tang, R. Zhao, S. Tang, and Z. Zeng, "Linear quadratic optimal control of a single-phase grid-connected inverter with an LCL filter," in *Proc. IEEE Int. Symp. Ind. Electron.*, May 2012, pp. 372–376.

Leandro Tomé Martins was born in Caxias do Sul, Rio Grande do Sul, Brazil, in 1992. He received the B.Sc. degree in control and automation engineering and the M.Sc. degree in electrical engineering, both from the Federal University of Santa Maria (UFSM), Santa Maria, Brazil, in 2015 and 2018, respectively. He is currently working toward the Dr.Eng. degree in electrical engineering with the UFSM.

His main research interests include modeling and control of static power converters, digital control techniques for power electronics, and control of grid-connected converters for distributed generation and renewable energy systems.

Márcio Stefanello (M'07) received the M.Sc. and Ph.D. degrees in electrical engineering from the Federal University of Santa Maria, Santa Maria, Brazil, in 2006 and 2010, respectively.

Since 2010, he has been a Professor with the Federal University of Pampa, Alegrete, Brazil. From 2016 to 2017, he was a visiting scholar with the Department of Electrical and Computer Engineering, Illinois Institute of Technology, Chicago, IL, USA. His current research interests include adaptive control, control of grid-connected converters, and microgrids.

Humberto Pinheiro (M'08) received the B.S. degree from the Federal University of Santa Maria (UFSM), Santa Maria, Brazil, in 1983, the M.Eng. degree in electrical engineering from the Federal University of Santa Catarina, Florianópolis, Brazil, in 1987, and the Ph.D. degree in electrical engineering from Concordia University, Montreal, QC, Canada, in 1999.

From 1987 to 1999, he was a Research Engineer with the Brazilian UPS company as well as a Professor in power electronics with the Pontifícia Universidade Católica do Rio Grande do Sul, Brazil. Since 1991, he has been with the UFSM. His research interests include modulation and control of static converters and drives and power converters for wind energy conversion systems.

Dr. Pinheiro is a member of the IEEE Power Electronics and IEEE Industrial Electronics Societies.

Rodrigo Padilha Vieira was born in Cruz Alta, Brazil. He received the B.S. degree in electrical engineering from the Universidade Regional do Noroeste do Estado do Rio Grande do Sul (Unijuí), Ijuí, Brazil, in 2007, and the M.Sc. and Dr. Eng. degrees in electrical engineering from the Federal University of Santa Maria (UFSM), Santa Maria, Brazil, in 2008 and 2012, respectively.

From 2010 to 2014, he was with the Federal University of Pampa, Alegrete, Brazil. Since 2014, he has been with the UFSM, where he is currently a Professor. His research interests include electrical machine drives, sliding-mode control, and digital control techniques of static converters.